IOP Publishing Nanotechnology
Nanotechnology 29 (2018) 365705 (11pp) https://doi.org/10.1088/1361-6528/aacba7

Controlled graphene encapsulation: a nanoscale shield for characterising single bacterial cells in liquid

Jiayao Li[1], Changxi Zheng[2], Boyin Liu[1], Tsengming Chou[3], Yeonuk Kim[1], Shi Qiu[1], Jian Li[4], Wenyi Yan[1] and Jing Fu[1,5,6]

[1] Department of Mechanical and Aerospace Engineering, Monash University, Clayton, VIC 3800, Australia
[2] Monash Centre for Atomically Thin Materials, Monash University, Clayton, VIC 3800, Australia
[3] Laboratory of Multiscale Imaging, Stevens Institute of Technology, Hoboken, NJ, United States of America
[4] Monash Biomedicine Discovery Institute, Department of Microbiology, Monash University, Clayton, VIC 3800, Australia
[5] ARC Centre of Excellence for Advanced Molecular Imaging, Monash University, Clayton, VIC 3800, Australia

E-mail: jing.fu@monash.edu

Received 9 March 2018, revised 20 May 2018
Accepted for publication 11 June 2018
Published 2 July 2018

Abstract

High-resolution single-cell imaging in their native or near-native state has received considerable interest for decades. In this research, we present an innovative approach that can be employed to study both morphological and nano-mechanical properties of hydrated single bacterial cells. The proposed strategy is to encapsulate wet cells with monolayer graphene with a newly developed water membrane approach, followed by imaging with both electron microscopy (EM) and atomic force microscopy (AFM). A computational framework was developed to provide additional insights, with the detailed nanoindentation process on graphene modelled based on the finite element method. The model was first validated by calibration with polymer materials of known properties, and the contribution of graphene was then studied and corrected to determine the actual moduli of the encapsulated hydrated sample. Application of the proposed approach was performed on hydrated bacterial cells (*Klebsiella pneumoniae*) to correlate the structural and mechanical information. EM and energy-dispersive x-ray spectroscopy imaging confirmed that the cells in their near-native stage can be studied inside the miniaturised environment enabled with graphene encapsulation. The actual moduli of the encapsulated hydrated cells were determined based on the developed computational model in parallel, with results comparable with those acquired with wet AFM. It is expected that the successful establishment of controlled graphene encapsulation offers a new route for probing liquid/live cells with scanning probe microscopy, as well as correlative imaging of hydrated samples for both biological and material sciences.

Supplementary material for this article is available online

Keywords: AFM, electron imaging, graphene, encapsulation, FEA

(Some figures may appear in colour only in the online journal)

1. Introduction

Progress in high resolution imaging and probing on liquid-phase specimens attracts increasing attention in various fields of biological science [1–3]. The new technologies offer unique insights into the dynamic processes and structures involved in live single cells. Electron microscopy (EM) on hydrated specimens has become feasible, due to the advances in silicon membrane technology. The existing approach includes SiN films, typically with thickness varying from 20

[6] Author to whom any correspondence should be addressed.

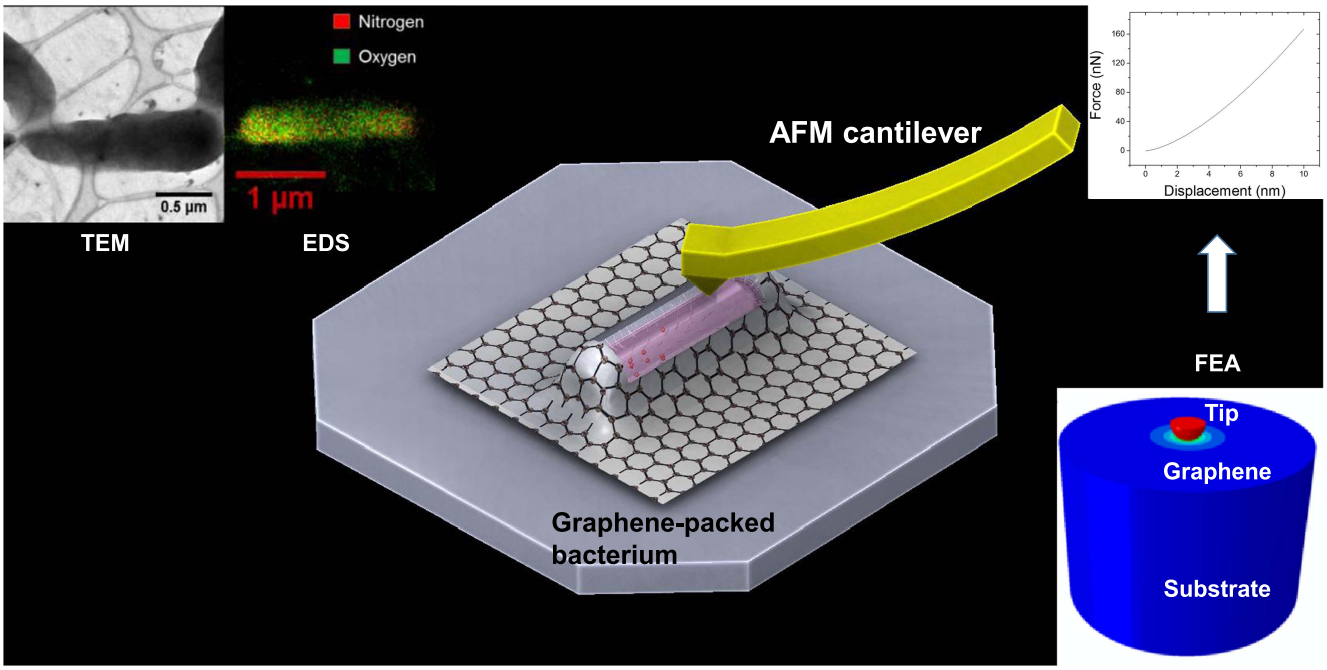

Figure 1. Schematic of the nanoindentation on graphene-packed bacterium with insets showing a transmission electron microscopy (TEM) image of a graphene-packed bacterial cell (*K. pneumoniae*), energy-dispersive x-ray spectroscopy (EDS) elemental maps and the constructed 3D finite element model, with modelled AFM tip indenting on graphene-bacteria composite. The corresponding force–displacement curve was simulated based on the computational framework to estimate the actual modulus of the hydrated cell.

to 100 nm, supported by silicon frames to achieve robust windows during imaging in vacuum [3]. However, when submicron resolution is desired, this approach is challenging as multiple objectives are to be met involving liquid thickness, window size and windows thickness [3]. As a matter of fact, both thicknesses of window and liquid layer underneath are expected to be less than 50 nm [3, 4]. These preferred thin windows, nevertheless, are unstable to remain in original geometry in high vacuum condition. As a result, the encapsulated liquid layer can increase by approximately 1 μm in thickness when the window deforms [5]. Furthermore, the SiN-film technology is not applicable to scanning probe microscopy (SPM) due to its layer thickness. For example, the force applied by the approaching atomic force microscopy (AFM) tip can only deform and displace the top SiN layer without breakage, while the actual hydrated sample surface remains undetected. On the other hand, the conventional AFM approach for scanning bacterial cells in liquid requires an additional fluid chamber [6], and the cells to be investigated need to be firmly attached to a substrate. Currently, physical adsorption, bacterium-coated AFM tip and mechanical trapping are the most frequently used strategies for cellular immobilisation [7]. While physical adsorption alters the physicochemical properties of the cellular surface, bacterium-coated AFM tip requires highly-skilled and time-consuming sample preparations [7]. Mechanical trapping, although proves to be the most reliable immobilisation method, is considered to be only applicable to spherical cells [7, 8].

As a potential solution to address the aforementioned issues, graphene, a material with superior mechanical properties and nanometre thickness, has been proposed to encapsulate biological cells and maintain a native environment during imaging and probing. Compared to the conventional approach that uses silicon membrane, graphene encapsulation keeps the hydrated samples almost transparent to the incident electrons with desired charge reduction and minimal electron scattering [9, 10]. The characteristics of being super-stiff and impermeable to any gases and liquids allow encapsulated samples to be investigated in a vacuum environment, a long-standing hurdle for electron imaging of hydrated sample at high resolution. For AFM applications with wet cells, sample preparation without any chemical treatment ensures the cellular surface to remain unmodified. It is also anticipated that graphene encapsulation is able to offer an improved immobilisation approach versatile for almost any cell shape due to that the size of graphene sheet currently available is larger than the sizes of common cell lines used in laboratories.

The trials of graphene (or graphene oxide) to 'wrap' bacteria for cellular imaging have been reported [11, 12], from which Deng *et al* [11] provided an approach for estimating the modulus of bacterial cell wall when studying the wrinkling effects of graphene. The approach utilises the Föppl −von Kármán equation where the wrinkle wavelength and pre-stretch factor have to be experimentally determined with both SPM and field emission scanning EM [11]. Such indirect measurement, however, could only offer a relatively coarse approximation after sample dehydration, and the calculated modulus is strongly dependent on the experimentally observed wrinkling details.

In the present study, direct measurement on the encapsulated sample has been proposed by coupling experiment

and simulation data, aiming to provide a repeatable and accurate evaluation on the moduli of graphene encapsulated samples (figure 1). The encapsulation approach has also been redesigned in this study, which effectively limited the occurring of wrinkles on graphene after encapsulation. Computational models for graphene encapsulation have been developed contrary to the previous wrinkling models. The particular focus is on the dynamics of nanoindentation process, with finite element analysis (FEA) executed to investigate the role of graphene in determining the actual moduli of the encapsulated cells. The quasi-static models between the graphene wrapped cell and an AFM tip are simulated, and the 'composite' model is recursively refined with the experiments performed with the encapsulation protocols developed. The protocols developed for graphene encapsulation and the computational framework allow exploring the fundamental mechanics involved in graphene encapsulation, as well as providing a unique solution for correlative high resolution imaging of hydrated cells with electrons and scanning probes.

2. Materials and methods

2.1. Sample preparation

Monolayer graphene film was grown on copper foil by chemical vapour deposition. A layer of Poly (methyl methacrylate) (PMMA) (Type A2, MicroChem, Westborough, USA) was spin-coated on the copper foil to protect the monolayer graphene grown on one side. The graphene layer grown on the other side was etched away by O_2 plasma to expose the copper surface. By leaving the clean copper surface on 0.1 M APS solution (Ammonia persulfate, Sigma Aldrich, Australia) for 3 h, the copper foil was etched away. The PMMA/graphene layer then was transferred to a beaker containing DI water for cleaning. A petri dish containing a piece of glass cover slip was applied to lift the PMMA/graphene layer. Excessive water was wicked away to form a thin water layer between graphene and the cover slip. Bacterial cells (*Klebsiella pneumoniae*) was prepared based on the same protocol used in [13]. Cells (ATCC 13883) were subcultured on agar plates, followed by being incubated in a shaking waterbath for overnight. Prior to the graphene encapsulation experiments, the cells were fixed with 2.5% glutaraldehyde (Sigma Aldrich, Australia) in phosphate-buffered saline (Sigma Aldrich, Australia) for 1 h, followed by the rinse with distilled water for three times. If required, the samples were stained with 1% Osmium Tetroxide (Sigma Aldrich, Australia) in water for 30 min, and rinsed with water for three cycles of 5 min each. A drop of bacterial solution was then injected into the thin water layer for encapsulation. Bacteria together with water were finally enclosed by the graphene film due to the adhesion caused by the subsequent dehydration, and the PMMA layer coated on graphene was removed by acetone. A series of schematic diagrams showing the detailed preparation steps are provided in the supplementary material 2, which is available online at stacks.iop.org/NANO/29/365705/mmedia.

2.2. AFM measurement

The force mapping experiments were carried out on AFM instrument (JPK NanoWizard II, JPK Instruments AG, Berlin, Germany). V-shaped cantilevers (SNL-10-D, Bruker, Billerica, USA) with nominal spring constant 0.06 N m^{-1} and quadratic silicon nitride pyramid shaped tip were employed. The nominal radius of the tip was 42 nm and half-open angle of the pyramidal face was 35° (RC800PB, Lever 2, Olympus, USA). Both the detector sensitivity (S) and the actual spring constant were calibrated before use [13]. A small area of cell surface was measured on both graphene wrapped and exposed cells. The force curves were collected for analysis using the JPK data processing software [14]. The measured force–distance curves included two segments: extend curve and retract curve. The extend curve was adopted to generate force–displacement (FD) curve as the contact point was masked in the retract curve due to adhesive interactions [14]. A series of force curve processing operations was performed including calibration of v-deflection, the subtraction of baseline offset, identifying the contact point, and calculating tip-sample separation. Such operations converted the force–distance curve into a force-depth curve, which was crucial since the displacement caused by piezo movement and cantilever deflection should be excluded [14, 15]. As a convention in this article, the actual measured depth in the original AFM data is referred to as *distance*, and after post-processing, the indentation depth is referred to as *displacement*. The moduli data were first calculated by fitting in the Hertz model. Settings for wet AFM measurements in water can be found in [13, 16].

2.3. TEM and EDS investigations

A 200 kV TEM (FEI CM20 FEG S/TEM, FEI Company, USA) equipped with a CCD camera (MSC 794 CCD camera, Gatan, Pleasanton, USA) was used to image the encapsulated bacterial cell in TEM mode. To study the elemental distribution of the bacterium, the microscope was operated in scanning mode (STEM mode). The Oxford Max-80 SDD EDS system (Oxford Instruments, Concord, USA) was used to collect the EDS maps.

2.4. Construction of finite element model

Modelling of the nanoindentation process was established as demonstrated in the geometries shown in figure 1, with the AFM tip modelled as the top half sphere. A cylinder of 600 nm diameter was constructed to represent the encapsulated material surface, and covered with a graphene layer of 0.5 nm in thickness. The height of the cylinder representing the underlying bacterium was set to 400 nm which was well beyond the average depth predicted in actual experiments. Diameter of the simulated area was 600 nm to ensure both the validity of continuous modelling [17, 18] and feasible computational time. The radius of AFM tip was based on the

specifications from the manufacturers. The mechanical properties required for the finite element model were sourced from either literature or manufacturer, with the only exception of encapsulated sample modulus which remained undetermined in the initial stage. Properties of materials used in the simulation were summarised in the supplementary material 1, and the AFM tip was assumed to be rigid. To attain greater computational efficiency and accuracy, the whole model was considered as a 2D axisymmetric model and quadratic meshes were constructed for the target material layer. Shell element was selected as the mesh element type for graphene considering the ultra-thin thickness. Mesh generated from the target material top layer was refined on normal direction to provide improved resolution. A mesh convergence study was first performed to ensure that results were independent of mesh size. Contact interactions were created between graphene-substance surfaces and tip-graphene surfaces. As suggested by previously reported studies [19–23], the surface-surface interactions involving graphene were assumed to be frictionless. It should be noted that in this study, water layer was not detected by either scanning electron microscope (SEM), TEM or AFM on top on the bacterial cells. Some liquid was observed only near the boundary profiles of some cells from top view by SEM where graphene started to separate from the cell. As such, no additional interface involving water layer was considered in the proposed simulation models, and this agreed with the current understanding of graphene interface in most recent studies as frictionless [21–23] or minimal friction coefficients ranging from 0.004 to 0.07 [24–26].

2.5. Numerical simulation

Numerical simulations were performed with a commercial package ABAQUS (version 6.14-1, Dassault Systems) in ABAQUS/Standard mode, with two major stages: (1) contact initialisation and (2) nanoindentation. In the first stage, a certain amount of initial displacement was applied on the tip, until the tip and graphene started to contact each other to avoid convergence issues. Typically, 10 nm displacement was applied in the following step where indentation took place, with bottom surface fixed in all directions. To prevent undesired rigid displacement, the tip movement was only allowed in normal direction in a quasi-static manner. In order to fully evaluate the effect caused by the addition of graphene on the FD curve, a parametric study was performed with varied modulus of target material. Scenarios including the cases with and without graphene layer were designed. Each of the two cases was repeatedly attempted with varied modulus of target material, typically ranging from 100 kPa to 800 MPa. Analyses were focused on the force and displacement in the normal direction, with a large number of simulations conducted in a semi-automatic manner. Scripts written in Python (version 2.7.6, Python Software Foundation) were compiled to perform the parametric study and post-processing. In post-processing, the maximum displacement on graphene-substance composite and the maximum force on tips were located and recorded at each time increment, which were then used to generate FD curves.

2.6. Model validation

The established model without graphene was first verified by applying the Hertz contact theory, a contact mechanic model that was developed for solving corresponding problems. For limited indentation, the solution for spherical model that describes elastic contact behaviour was adopted where an isotropic sphere indented a half-space [27, 28]. The implementation of the Hertz approximation analytically determined the modulus from FD curve. Detailed Hertz equation is listed below, where F, R_c, E, ν, and δ refer to force, radius of tip, Young's modulus, Poisson's ratio, and depth of indentation, respectively [27, 28]

$$F = \frac{4\sqrt{R_c}}{3}\frac{E}{1-\nu^2}\delta^{\frac{3}{2}}. \quad (1)$$

Regression analysis was conducted, from which FD curves obtained from simulations were fitted by this correlation to assess the elastic modulus of the sample.

For the scenarios without the graphene layer, the calculated moduli of the encapsulated samples were used to compare with the initially assumed ones, and models were considered as validated if results agreed with each other [29]. To compare the variation of modulus due to graphene, the moduli data of graphene-substance composite were also fitted by the Hertz theory. It should be noted that the Hertz theory is a coarse approximation considering the anisotropic properties of graphene. In our study, this approximation provided a reasonable reference to quantitatively compare the contribution of graphene encapsulation.

In addition, the computational model of graphene-substance composite was experimentally verified by introducing a reference/calibration sample of polydimethylsiloxane (PDMS) with known modulus. Nanoindentation experiments were conducted on both PDMS and graphene-packed PDMS prepared with the same steps of cell encapsulation, and the acquired FD relationships were then compared side-by-side with the simulation results from FEA.

2.7. Predicting mechanical properties after graphene encapsulation

With constructed liquid environment accessories, a conventional AFM or other nanoindentation can be further equipped to probe hydrated cells [30–34]. The graphene approach developed in this study provides a straightforward alternative: a local miniature liquid environment, and the FEA model established in this study helps determine the actual moduli of hydrated cells without sophisticated accessories. In a previous study on mechanics, Hay *et al* [35] have proposed that the properties of covered substrate could be extracted by performing both FEA and experimental indentation studies, provided that properties of the covering film were known. This method requires a reasonable estimation of the substrate modulus to initiate simulation, and the initial modulus is then

recursively adjusted until matching the FD data [35]. In this study, assessment on the moduli of wrapped samples were achieved using similar routines including the least squares method. The AFM measured FD data of the 'graphene composites' were fitted to a series of numerically simulated data based varied modulus of the encapsulated samples. The actual moduli of the encapsulated samples (cells) were determined based on the best matches of simulated and experimental FD data.

3. Results and discussion

3.1. Electron and scanning probe imaging of graphene encapsulated cells

Bacterial cells (*K. pneumoniae)* on Holey carbon TEM grid were 'sandwiched' with two graphene layers, while single cells were successfully wrapped in hydrated state in some areas. An acquired TEM image (figure 2(a)) from the cell envelope of an unstained cell encapsulated shows even-layered structures, which can typically only be revealed with cryo-TEM [36, 37]. AFM topologic map (figure 2(b)) acquired from the same type of cells prepared on Si wafer in parallel showed comparable morphology compared to a map acquired with liquid environment AFM (wet AFM). It should be noted that no significant extra information on top of the cell surface has been revealed with wet AFM, although the acquired map from the wrapped cells appears to be a smoother surface due to the graphene layer on top. High contrast of the cell boundary in figure 2(b) suggest some loss of details when probing the curved surface around the graphene wrapped cells, compared to the acquired map with wet AFM (figure 2(c)).

A summary of the EDS mapping on graphene encapsulated cells and the control samples is presented in figures 2(d)–(g). Low magnification TEM images have been first acquired to locate the target cells, and clearly the morphologies of cells are well preserved with graphene encapsulation (figures 2(d) and (e)). In the acquired maps, the elements appear to be more uniformly distributed within the wrapped cells (figures 2(d) and (e)) compared to the air dried controls (figures 2(f) and (g)). One notable finding is the excessive carbon signals detected after graphene encapsulation in figures 2(d) and (e). It is likely that the graphene layers and the Holey carbon film prefabricated on TEM grid have contributed to the signals of carbon, and thus interpretation of carbon data requires additional caution in the future. No other excessive patterns have been observed in the acquired elemental maps. Particularly for oxygen and phosphorous in the graphene wrapped cells, reduced signals have been revealed from at the two ends of each cell. In a previous structural study on *K. pneumoniae* [16], distinct large granules have been discovered at the two ends with electron tomography on resin embedded cells. Results from this study suggest that these granules have reduced compositions of O and P compared to the average intracellular domain. The disordered maps acquired from the control samples (figures 2(f) and (g)), possibly due to the damages during dehydration, have offered minimal insights.

3.2. Modulus model validation

In addition to imaging for which the ultra-thin graphene has provided many advantages, the proposed encapsulation approach maintains the cells in their native or near-native state and provides unique opportunities to explore the mechanical signatures of cells. The extraordinary mechanical properties of graphene, although providing sample protection, can possibly alter the deformation during measurements such as nanoindentation. An FEA model is established to understand the details, and to validate this model, FD curves derived from the simulation results of no-graphene cases were first fitted by the Hertz equation (1). Comparisons were made between the assumed modulus values and those evaluated by the Hertz theory. As stated in section 2.6, modulus was assessed by curve fitting based on the contact region of the FD curve. As illustrated in figure 3(a), a tip displacement of 10 nm was predefined, and applied forces in an increasing order were either simulated from the FE model or calculated with the Hertz theory. A close match is found with an average error of 2.3% from all the data points, and this error value appears to be independent of the material modulus. A comparison of the fitted moduli from FEA with the predefined material modulus (500 MPa) shows a deviation of 1.4% based on the FD curve when indentation depth is from 0 to 4 nm (2.5% deviation if using curve 0–10 nm). In the following section, FD curve regions with 0–4 nm depth were used for all the curve fitting.

PDMS was chosen as a reference sample to validate the accuracy of simulated force-depth relation particularly for graphene encapsulation. AFM measurements were performed on the prepared flat PDMS samples to acquire FD curves. The average modulus of PDMS was determined to be 12.32 MPa by fitting the experimentally acquired FD curves (contact region) to the Hertz equation (1). As detailed in figure 3(b), the simulation results agree with the experimental data shown in dots, and the FD curve measured by AFM (dotted) appears between the two simulated FD curves with assumed sample modulus of 10 and 20 MPa. The same comparison was repeated on the same batch of PDMS covered with graphene. Significant larger forces are required to result in the same indentation depth due to the stiffness of the graphene, while both experimental and simulate curves confirm this (figure 3(c)). It should be noted that some twisted sections have been observed in the experimentally measured FD curve from displacement of 1.5 nm (figure 3(c)), which are potentially due to sliding occurred between the frictionless/near-frictionless graphene surface and the PDMS surface. The overall curve, however, still agree well with the simulated FD curves with sample modulus from 10 to 20 MPa. This suggests that the constructed simulation properly models the indentation process on graphene, and will be capable of estimating the modulus of graphene-covered substrate.

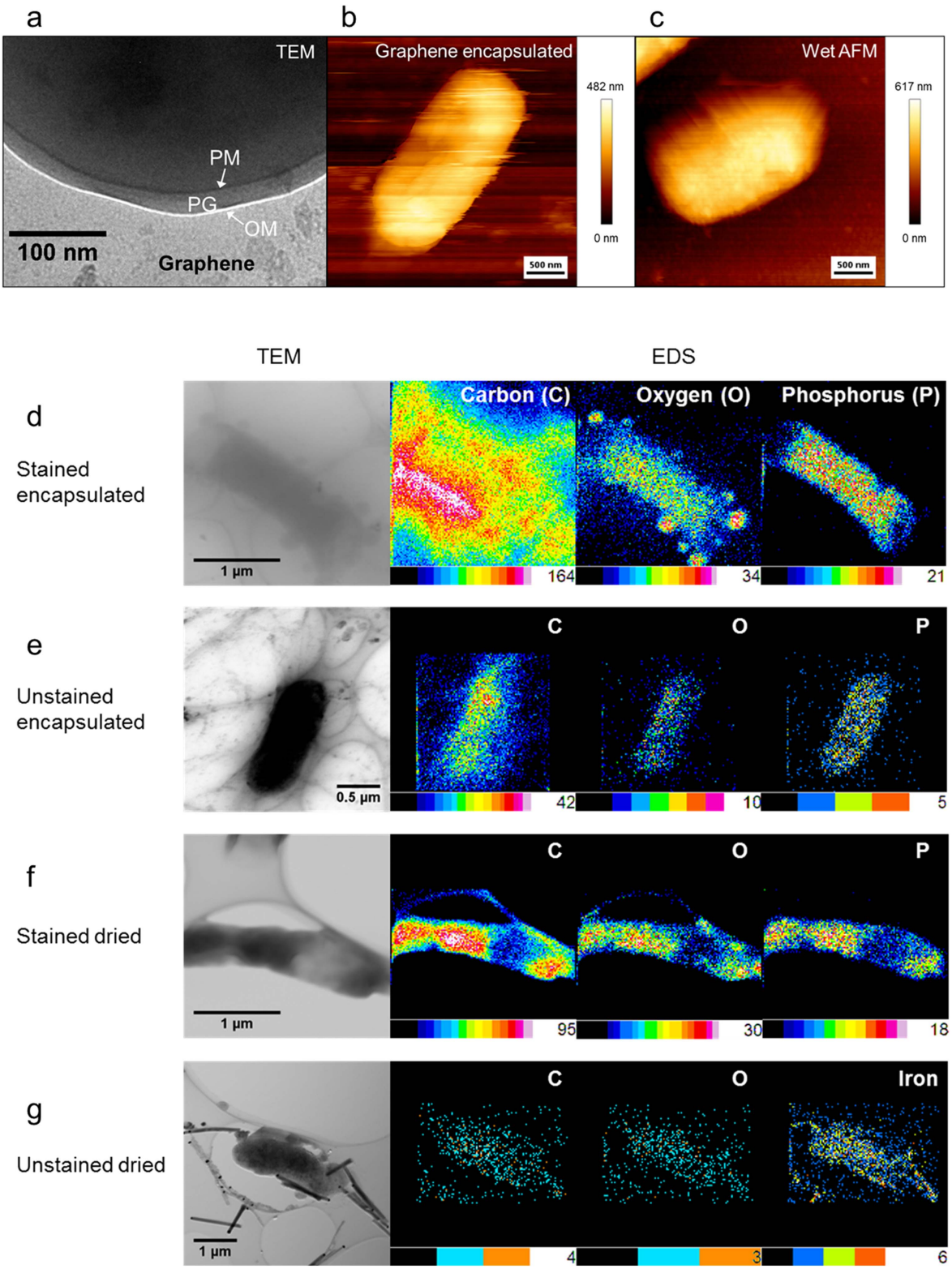

Figure 2. (a) TEM image acquired from a glutaraldehyde-fixed and unstained bacterial cell (*K. pneumoniae*) after graphene encapsulation (OM: outer membrane; PG: peptidoglycan layer; PM: plasma membrane); (b) AFM topologic maps acquired on the same hydrated bacterial cells on silicon after graphene encapsulation, compared to (c) topologic map of a control hydrated cell acquired by AFM with liquid environment accessary (wet AFM). EDS elemental maps acquired from (d) stained and (e) unstained *K. pneumoniae* cells encapsulated by two graphene layers prepared on Holey carbon TEM grids, with (f) and (g) control samples air dried without graphene encapsulation. The colour bars in (d)–(g) each represent the normalised number (count) of detected x-rays within a specific energy range which is associated with an element, along with the maximum number of counts displayed on the right.

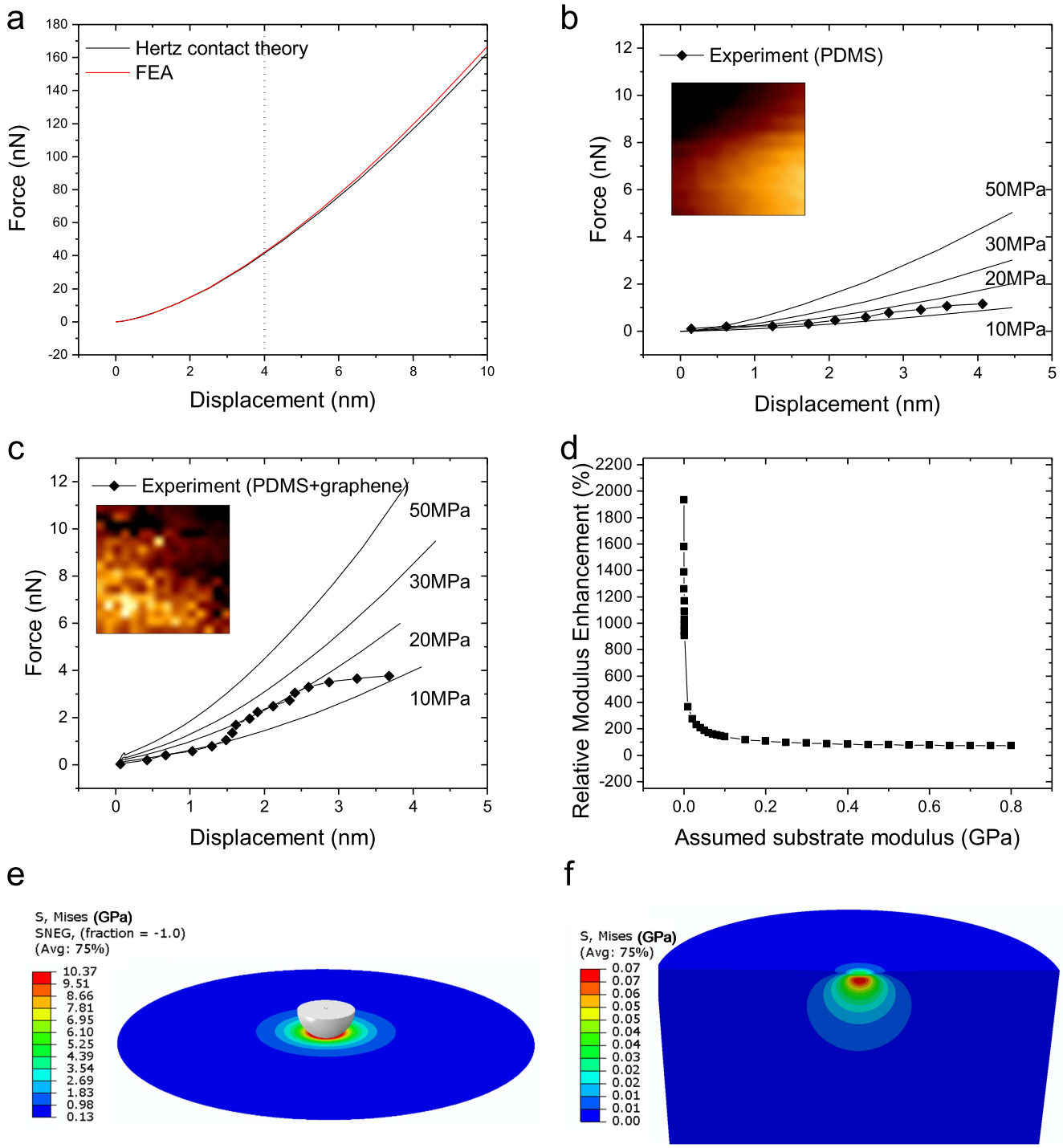

Figure 3. (a) Comparison of FD curves based on the Hertz contact theory and the developed FEA simulation for a predefined materials (500 MPa) without graphene encapsulation. Force-depth relations of PDMS and target materials of varied modulus (b) without graphene encapsulation and (c) with graphene, acquired in parallel by AFM force spectroscopy (dotted curve) and FEA, (d) based on the Hertz model, changes (enhancement) of measured moduli resulted from encapsulation of graphene on target materials with varied actual moduli. Simulation of the nanoindentation process resulted in (e) the deformed graphene layer and (f) a cross-sectional view of the indented encapsulated materials with $E = 500$ MPa. Insets in (b) and (c) show the corresponding acquired force maps.

3.3. Modulus prediction of graphene encapsulated sample

The schematics of the deformed model of simulated graphene-substrate composite are illustrated in figures 3(e) and (f). The reference point on the tip model initially approached the centre point on graphene surface. With continuously applied displacement, the contact area increased and a circular-shaped dent was observed. As revealed in figure 3(f), the centre denting area possesses the largest stress. The stress is distributed to a limited area whereas the surrounding regions remain stress-free. The maximum stress (10.37 GPa)

resulted from the 10 nm indentation appears to be in the graphene layer, comparable to the maximum stress (0.07 GPa) imposed on the encapsulated sample of pre-assumed modulus of 500 MPa. Such significant difference suggests that the graphene after successful encapsulation can provide a strong controllable layer to prevent damage on cells, yet it is also sufficiently flexible for modulus calculation. The results reveal that FD curves have been distinctly changed with the addition of a graphene layer. Significant enhancement on modulus is detected, as shown in figure 3(d). With the assumed modulus of bacteria ranging from 100 kPa to 0.8 GPa, the enhancement of modulus resulted from graphene encapsulation can be varied; from 1932.7% at 100 kPa to 73.2% at 0.8 GPa. The results also imply that stiffer biological materials wrapped by graphene result in less increase of modulus as reflected when measuring the 'graphene composite'.

3.4. Simulation of water layer in graphene encapsulation

Based on the FEA in this study, detailed 'engineering' charts containing curves from nanoindentation on covered material of varied modulus were constructed as illustrated in figures 4(b) and (c). An FD curve acquired on graphene encapsulated materials was promptly fitted to the chart to determine the actual modulus. A typical example is provided, in which the modulus of hydrated *K. pneumoniae* cells was assessed based on the computation models developed. Topologies on both the hydrated single-cell with/without graphene encapsulation were acquired by AFM measurements (figures 2(b) and (c)). The local surface roughness of the hydrated cell is found to be essentially flat, indicated by an approximately 10 nm surface roughness, which is consistent with the assumption of flat top surface made on constructing FEA model of the encapsulated substrate. Figure 4(a) illustrates the AFM topology and its corresponding force–distance curve for another encapsulated hydrated cell. The AFM tip first moves towards the target surface and then comes into contact with the surface, followed by the occurrence of indentation highlighted as the bold straight line in figure 4(a). This line is located in the contact region and utilised for modulus determination. In this study, least squares method was used to determine the closest FD curve from the database (figures 4(b) and (c)), to reversely determine the actual modulus of graphene wrapped samples. Comparison between the FD curves sourced from FEA results and experimental data (*K. pneumoniae*) are presented in figure 4(b). Further parametric studies were performed by varying the sample modulus from 100 to 300 kPa, with reduced step size of 10 kPa. Indicated by the data fitting results, the actual modulus of the cell measured is approximately to be 140 kPa, comparable with wet AFM results and previous experiment measurements [13]. Without the proposed computational framework, the composite modulus will be incorrectly calculated if solely based on the Hertz model, as the assumption of isotropic material is no longer valid. Further estimation of the wrapped-material modulus will be also incorrect using the current models developed for a film-substrate system [28, 35].

For preparing the encapsulation of biological samples, water interface between the graphene layer and the underlying samples, however, cannot be excluded. Although no clear water interface has been observed in the bacterial application in this research, the scenario with additional water layer was also simulated to gain a deeper insight into its effects during such quasi-static nanoindentation process. Smoothed particle hydrodynamics (SPH) was used to simulate the behaviour of hydrostatic water that interacts with solid [38]. In this approach, the meshless feature that discretises elements into particles is applicable for large 3D deformations. Compared with another computational method (coupled Eulerian–Lagrangian) that is also frequently used for simulating solid–liquid interaction, SPH exhibits competitive advantage of being more computationally effective, especially for this nanoscale model as such 3D simulation takes huge amount of time. More details of the water interface simulation method are summarised in the supplementary material 3.

Quasi-static nanoindentation on a 50 MPa substrate encapsulated by graphene was simulated with a newly added water interface of 5 nm or 10 nm in thickness. As shown in the results (supplementary animation 1 and 2), the majority of water particles underneath the contact region are slowly squeezed out by the moving AFM tip. Indicated by figure 4(d), the resultant FD curves illustrate altered patterns compared with the one previously simulated without water interface. The resultant FD curves initially remain relatively flat, and it rapidly ascends when tip approaching certain displacements. The rapidly increasing sections appear to be the same to that from the case without water interface. The initially flat sections are believed to be mainly the indentation of water layer. The initial applied force forces the water to leave the tip contacting zone, with minimal effects on the graphene layer and the underlying samples as revealed in the simulation results. After the removal of a certain amount of water, the underlying sample surface commences to deform, as shown by the rapid increasing FD curve. The intermediate water layer, if present, would shift the FD curves to the right (figure 4(d)). By recognising this shifts, the effects of possible water layer can be minimised, with the interactions among tip, graphene, and cell remain the same in the proposed simulation framework.

4. Conclusion and future development

The successful establishment of both experimental protocols and modelling provides an innovative approach on probing liquid/live cells with improved resolution and higher accuracy. In addition to EDS, chemical mapping of cells approaches such as electron energy loss spectroscopy [39, 40], secondary ion mass spectrometry [41], and atom probe tomography [42, 43] require a high vacuum environment, and graphene has been proved to be sufficiently strong during EDS mapping in this study. Both encapsulation of cells on Si and two graphene layer encapsulation on TEM grid have been demonstrated in this study, and these can be directly adopted by the chemical mapping approaches listed above.

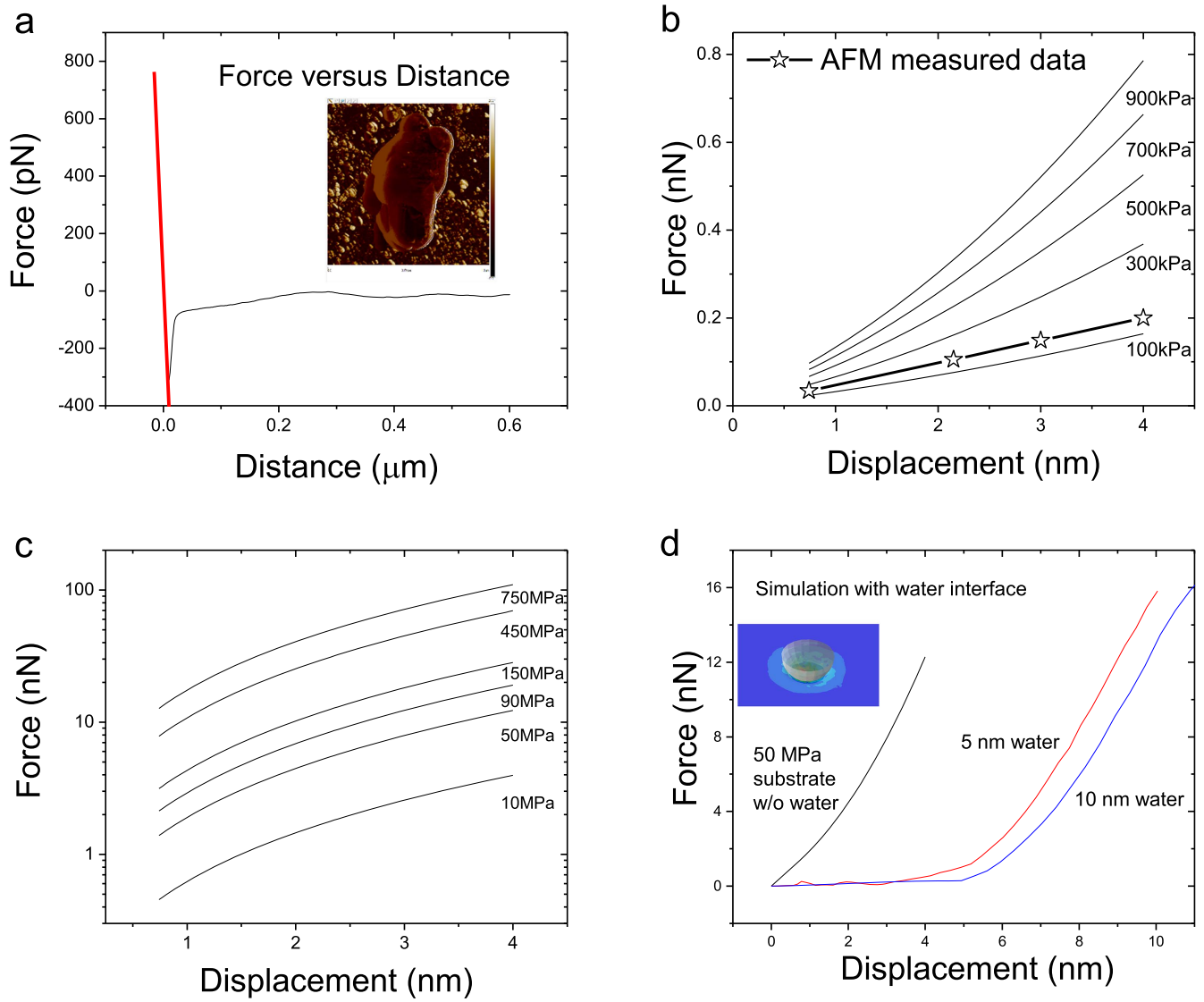

Figure 4. (a) Experimental FD curve acquired by AFM and AFM image taken on hydrated *K. pneumonia* after graphene encapsulation. Simulated force–displacement curves of indentation on graphene encapsulated samples of modulus ranges in (b) 100–900 kPa with experimental data curves fitted at 140 kPa, and (c) simulated curves of graphene encapsulated sample modulus from 10 to 750 MPa. (d) Simulated FD curves with a water layer between the graphene and encapsulated substance (50 MPa), with varied thickness of 0 nm (no water layer), 5 nm and 10 nm, (inset: FEA model showing the indentation on water layer).

Compared with the conventional cell immobilisation approach applied in AFM imaging in liquid that involves poly-L-lysine [19, 34, 44, 45], graphene encapsulation exhibits improved characteristics including lower cost (graphene preparation versus additional AFM liquid environment cost) [12], higher durability with regard to the frequent damages caused by tip contact [12], and enhanced electrical sensitivity [45]. The FD patterns in conjunction with the modelling provide an effective method to explore the elastic behaviour of soft materials and cells at micro/nanoscale.

This study has constructed the first computational framework for detailed modelling the process of probing graphene encapsulated soft materials. Through the constructed finite element models, reaction forces exerted during indentation were simulated based on the tip displacement. Noticeable alterations on the patterns of FD curves have been observed with the newly added graphene layer, and as a result, the enhancement on the overall composite modulus can be concluded as significant. The simulation model constructed was applied to determine the actual modulus of encapsulated hydrated bacterial cells, achieved by least squares method with varied pre-assumed bacterial modulus. Parameters set in the computational model were in accordance to the actual ones in the nanoindentation process, in which the hydrated bacterial cells immobilised and wrapped by an ultra-smooth graphene layer were probed by the AFM tip. The compiled engineering charts of the simulated FD curves have also been provided as a reference for future modulus determination after graphene encapsulation.

To determine the actual modulus of wrapped wet/live cell more efficiently, future efforts are needed to explore the physical behaviours of graphene encapsulated samples with

different types of AFM tips. An analytical or empirical model is expected for estimating the underlying modulus quickly by offsetting contributions of tip geometry. The current study did not consider the surface roughness on bacterial cells, as well as its effects on simulation and modelling. However, indicated by AFM topology of the provided bacterial cells, cellular surfaces were found to be practically flat, by comparing with the radius of the applied AFM tip (∼40 nm). As such, the effects of surface roughness are considered to be minimal in the established models of this study. A pre-assessment by high resolution SEM, TEM, AFM or focused ion beam tomography technique [16, 46] can provide some knowledge of actual surface details which can be an input in the simulation model. It is anticipated that the proposed approach possesses the potential capability for precisely tracking both the morphological and physical changes of 'superbugs' during the uptake of antibiotics, providing a better understanding in drug-cell interactions [13, 47, 48].

Acknowledgments

This study was partly funded by the Australian Research Council (DP180103955) and the Australian National Health & Medical Research Council (APP1046561). Jiayao Li is supported by Australian Government Research Training Program scholarship and PhD top-up scholarship from Monash Centre for Atomically Thin Materials (MCATM). Changxi Zheng thanks support from ARC DECRA (DE140101555). Jian Li is supported by a research grant from the National Institute of Allergy and Infectious Diseases of the National Institutes of Health (R01 AI132681 and AI132154). The content is solely the responsibility of the authors and does not necessarily represent the official views of the National Institute of Allergy and Infectious Diseases or the National Institutes of Health. Jian Li is an Australian NHMRC Senior Research Fellow. This work was performed in part at the Melbourne Centre for Nanofabrication (MCN), Victorian Node of the Australian National Fabrication Facility (ANFF). Also, the authors acknowledge use of facilities within the Monash Centre for Electron Microscopy (MCEM) and Monash Campus Cluster (MCC).

ORCID iDs

Jian Li https://orcid.org/0000-0001-7953-8230
Jing Fu https://orcid.org/0000-0002-7752-5417

References

[1] Horber J and Miles M 2003 Scanning probe evolution in biology *Science* **302** 1002
[2] Bogner A, Jouneau P H, Thollet G, Basset D and Gauthier C 2007 A history of scanning electron microscopy developments: towards 'wet-STEM' imaging *Micron* **38** 390–401
[3] de Jonge N and Ross F M 2011 Electron microscopy of specimens in liquid *Nat. Nanotechnol.* **6** 695–704
[4] Peckys D B, Veith G M, Joy D C and de Jonge N 2009 Nanoscale imaging of whole cells using a liquid enclosure and a scanning transmission electron microscope *PLoS One* **4** e8214
[5] Ring E A and de Jonge N 2012 Video-frequency scanning transmission electron microscopy of moving gold nanoparticles in liquid *Micron* **43** 1078–84
[6] Eaton P and West P 2010 *Atomic Force Microscopy* (Oxford: Oxford University Press)
[7] Vadillo-Rodríguez V, Busscher H J, Norde W, De Vries J, Dijkstra R J, Stokroos I and Van Der Mei H C 2004 Comparison of atomic force microscopy interaction forces between bacteria and silicon nitride substrata for three commonly used immobilization methods *Appl. Environ. Microbiol.* **70** 5441–6
[8] El Kirat K, Burton I, Dupres V and Dufrene Y 2005 Sample preparation procedures for biological atomic force microscopy *J. Microsc.* **218** 199–207
[9] Pantelic R S, Suk J W, Magnuson C W, Meyer J C, Wachsmuth P, Kaiser U, Ruoff R S and Stahlberg H 2011 Graphene: substrate preparation and introduction *J. Struct. Biol.* **174** 234–8
[10] Sader K, Stopps M, Calder L J and Rosenthal P B 2013 Cryomicroscopy of radiation sensitive specimens on unmodified graphene sheets: reduction of electron-optical effects of charging *J. Struct. Biol.* **183** 531–6
[11] Deng S, Gao E, Wang Y, Sen S, Sreenivasan S T, Behura S, Kral P, Xu Z and Berry V 2016 Confined, oriented, and electrically anisotropic graphene wrinkles on bacteria *ACS Nano* **10** 8403–12
[12] Akhavan O, Ghaderi E and Esfandiar A 2011 Wrapping bacteria by graphene nanosheets for isolation from environment, reactivation by sonication, and inactivation by near-infrared irradiation *J. Phys. Chem.* B **115** 6279–88
[13] Liu B, Uddin M H, Ng T W, Paterson D L, Velkov T, Li J and Fu J 2014 *In situ* probing the interior of single bacterial cells at nanometer scale *Nanotechnology* **25** 415101
[14] JPK instruments AG 2012 JPK data processing software manual edition 4.2 (accessed 25th June 2018)
[15] Baniasadi M, Xu Z, Gandee L, Du Y, Lu H, Zimmern P and Minary-Jolandan M 2014 Nanoindentation of pseudomonas aeruginosa bacterial biofilm using atomic force microscopy *Mater. Res. Express* **1** 045411
[16] Liu B, Heidi H Y, Ng T W, Paterson D L, Velkov T, Li J and Fu J 2014 Nanoscale focused ion beam tomography of single bacterial cells for assessment of antibiotic effects *Microsc. Microanal.* **20** 537–47
[17] Chandramouli P N 2011 *Engineering Mechanics* (India: PHI Learning)
[18] Yan W, Sun Q, Feng X-Q and Qian L 2007 Analysis of spherical indentation of superelastic shape memory alloys *Int. J. Solids Struct.* **44** 1–17
[19] Raman A, Trigueros S, Cartagena A, Stevenson A, Susilo M, Nauman E and Contera S A 2011 *Nat. Nanotechnol.* **6** 809–14
[20] Berry V 2013 Impermeability of graphene and its applications *Carbon* **62** 1–10
[21] Mi B 2014 Graphene oxide membranes for ionic and molecular sieving *Science* **343** 740–2
[22] Liu G, Jin W and Xu N 2015 Graphene-based membranes *Chem. Soc. Rev.* **44** 5016–30
[23] Min S K, Kim W Y, Cho Y and Kim K S 2011 Fast DNA sequencing with a graphene-based nanochannel device *Nat. Nanotechnol.* **6** 162–5
[24] Filleter T, McChesney J L, Bostwick A, Rotenberg E, Emtsev K, Seyller T, Horn K and Bennewitz R 2009 Friction and dissipation in epitaxial graphene films *Phys. Rev. Lett.* **102** 086102

[25] Lee C, Wei X, Li Q, Carpick R, Kysar J W and Hone J 2009 Elastic and frictional properties of graphene *Phys. Status Solidi* b **246** 2562–7
[26] Shin Y J, Stromberg R, Nay R, Huang H, Wee A T, Yang H and Bhatia C S 2011 Frictional characteristics of exfoliated and epitaxial graphene *Carbon* **49** 4070–3
[27] Lin D C, Dimitriadis E K and Horkay F 2007 Robust strategies for automated AFM force curve analysis: I. Non-adhesive indentation of soft, inhomogeneous materials *J. Biomech. Eng.* **129** 430–40
[28] Yan W, Sun Q, Feng X-Q and Qian L 2006 Determination of transformation stresses of shape memory alloy thin films: a method based on spherical indentation *Appl. Phys. Lett.* **88** 241912
[29] Yan W and Fischer F 2000 Applicability of the Hertz contact theory to rail-wheel contact problems *Arch. Appl. Mech.* **70** 255–68
[30] Shao Z, Mou J, Czajkowsky D M, Yang J and Yuan J 1996 Biological atomic force microscopy: what is achieved and what is needed *Adv. Phys.* **45** 1–86
[31] Radmacher M, Fritz M, Kacher C M, Cleveland J P and Hansma P K 1996 Measuring the viscoelastic properties of human platelets with the atomic force microscope *Biophys. J.* **70** 556–67
[32] Li Q, Lee G, Ong C and Lim C 2008 AFM indentation study of breast cancer cells *Biochem. Biophys. Res. Commun.* **374** 609–13
[33] Dufrene Y 2001 Application of atomic force microscopy to microbial surfaces: from reconstituted cell surface layers to living cells *Micron* **32** 153–65
[34] Henderson E 1994 Imaging of living cells by atomic force microscopy *Prog. Surf. Sci.* **46** 39–60
[35] Hay J and Pharr G 2000 *Instrumented Indentation Testing* (Novelty, OH: ASM international)
[36] Zuber B, Chami M, Houssin C, Dubochet J, Griffiths G and Daffé M 2008 Direct visualization of the outer membrane of mycobacteria and corynebacteria in their native state *J. Bacteriol.* **190** 5672–80
[37] Hoffmann C, Leis A, Niederweis M, Plitzko J M and Engelhardt H 2008 Disclosure of the mycobacterial outer membrane: cryo-electron tomography and vitreous sections reveal the lipid bilayer structure *Proc. Natl Acad. Sci.* **105** 3963–7
[38] Dassault Systemes Simulia Corporation 2014 Abaqus 6.14 documentation (accessed 26th June 2018)
[39] Aronova M A and Leapman R D 2012 Development of electron energy-loss spectroscopy in the biological sciences *MRS Bull.* **37** 53–62
[40] Aronova M A, Kim Y C, Harmon R, Sousa A A, Zhang G and Leapman R D 2007 Three-dimensional elemental mapping of phosphorus by quantitative electron spectroscopic tomography (QuEST) *J. Struct. Biol.* **160** 35–48
[41] Passarelli M K and Ewing A G 2013 Single-cell imaging mass spectrometry *Curr. Opin. Chem. Biol.* **17** 854–9
[42] Narayan K, Prosa T J, Fu J, Kelly T F and Subramaniam S 2012 Chemical mapping of mammalian cells by atom probe tomography *J. Struct. Biol.* **178** 98–107
[43] Adineh V R, Marceau R K W, Velkov T, Li J and Fu J 2016 Near-atomic three-dimensional mapping for site-specific chemistry of 'superbugs' *Nano Lett.* **16** 7113–20
[44] Doktycz M, Sullivan C, Hoyt P, Pelletier D, Wu S and Allison D 2003 AFM imaging of bacteria in liquid media immobilized on gelatin coated mica surfaces *Ultramicroscopy* **97** 209–16
[45] Zhang D, Zhang Y, Zheng L, Zhan Y and He L 2013 Graphene oxide/poly-l-lysine assembled layer for adhesion and electrochemical impedance detection of leukemia K562 cancercells *Biosens. Bioelectron.* **42** 112–8
[46] Abuelfilat A, Kim Y, Miller P, Hoo S, Li J, Chan P and Fu J 2015 Bridging structure and mechanics of three-dimensional porous hydrogel with x-ray ultramicroscopy and atomic force microscopy *RSC Adv.* **5** 63909–16
[47] Azad M A, Roberts K D, Yu H H, Liu B, Schofield A V, James S A, Howard D L, Nation R L, Rogers K and de Jonge M D 2015 Significant accumulation of polymyxin in single renal tubular cells: a medicinal chemistry and triple correlative microscopy approach *Anal. Chem.* **87** 1590–5
[48] Bolshakova A, Kiselyova O, Filonov A, Frolova O Y, Lyubchenko Y L and Yaminsky I 2001 Comparative studies of bacteria with an atomic force microscopy operating in different modes *Ultramicroscopy* **86** 121–8